Size Control of CdS Nanocrystals in Block Copolymer Micelle

Dayang Wang,* Yaan Cao, Xintong Zhang, Zhiqiang Liu, Xinming Qian, Xin Ai, Fengqi Liu, Dejun Wang, Yubai Bai, Tiejin Li, and Xinyi Tang

Department of Chemistry, Jilin University, Changchun, 130023, Peoples Republic of China

Received September 8, 1998. Revised Manuscript Received November 23, 1998

In hydroxylated poly(styrene-*b*-butadiene-*b*-styrene) (HO-SBS) micelle, a series of CdS nanocrystals with different sizes have been prepared by means of simply repeating the synthesis procedure for a definite number of cycles. A variety of techniques including element analysis, infrared spectroscopy (IR), transmission electron microscopy (TEM), UV−visible spectroscopy, surface photovoltage spectroscopy (SPS), and electric field induced surface photovoltage spectroscopy (EFISPS) had been used for the characterization of the resulting CdS/HO-SBS nanocomposites. A reasonable energy band model was supposed to describe the electron process in the nanocomposites.

1. Introduction

Nanocrystals have a dimensions, as their name implies, in 1−100 nm. They possess an identical interior, structurally identical with the corresponding bulk solid, with a substantial fraction of the total number of atoms on the surface. Quantum states in the nanocrystals are size-dependent, leading to new electronic, optical, magnetic, catalytic, and mechanical properties. The area of application that can be foreseen to benefit from the small size and self-organization of nanocrystals includes nanoelectronics, nonlinear optics, catalysis, high-density information storage, and hybrid materials.[1−4] So far, nanocrystals can be prepared by a wide range of synthetic methods, e.g. CdS(Se).[2,5−12]

As the promising application of nanocrystals is coming true, films and fibers are of great interest as the final application form. For this reason, the good processability and large stability of nanocrystals is necessary. Nanocomposite techniques provide a new method to improve the processability and stability of nanocrystals with intriguing novel electronic, optical, and magnetic capacities.[13] The general principles in the construction of nanocomposites involve the intimate mixing of nanocrystals with processable matrixes. The matrix materials include polymers, glasses, or ceramics. Particulate phases nanocrystals can be prepared by means in situ or ex situ.[14,15]

Under nearly equilibrium conditions, A/B block copolymers can self-organize into a variety of nanosized microphase separation structures, depending on the A block volume fraction (f_a), Flory−Huggings parameter (χ), and polymerization degree.[16−19] Recently, the construction of nanocomposites by using block copolymers has been inspired by their self-organization nanostructures.[20−22] The nanopatterned polymer matrixes provide spatially localized sites for nucleation, minimize the degree of particle aggregation, and impose an upper limit on their size. On the other hand, block copolymers tend to self-organize in selective solvents, forming aggregates that are structurally analogous to micelles of associated surfactant molecules. Such micelles consist of an insoluble block core and a soluble shell. The driving force for micellization is generally attributed to microphase precipitation of the insoluble blocks although the final structure of the micelle is an expression of both enthalpic and entropic factors.[23−25] Furthermore, the critical micelle concentration of block copolymers is typically smaller and their kinetic stability is larger than that of low molecular weight surfactants. Block copolymers with such core-forming blocks as poly (2-

(1) Brus, L. *J. Phys. Chem.* **1986**, *90*, 2555.
(2) Wang, Y.; Herron, N. *J. Phys. Chem.* **1991**, *95*, 525.
(3) Weller, H. *Adv. Mater.* **1993**, *5*, 88.
(4) Alivisatos, A. P. *Science* **1996**, *271*, 933.
(5) Steigerwald, M. L.; Alivosatos, A. P.; Gibson, J. M.; Harris, T. D.; Kortan, R.; Muller, A. M.; Thayer, A. M.; Duncan, T. M.; Douglus, D. C.; Brus, L. E. *J. Am. Chem. Soc.* **1988**, *110*, 3046.
(6) Watzke, H. J.; Fendler, J. H. *J. Phys. Chem.* **1987**, *91*, 854.
(7) Resch, U.; Eychmüller, A.; Haase, M.; Weller, H. *Langmuir* **1992**, *8*, 2215.
(8) Choi, K. M.; Shea, K. J. *Chem. Mater.* **1993**, *5*, 1067.
(9) Murray, C. B.; Kagan, C. R.; Bawendi, M. G. *Science* **1995**, *270*, 1335.
(10) Wong, Kim K. W.; Mann, S. *Adv. Mater.* **1996**, *8*, 928.
(11) Braun, P. V.; Osenar, P.; Stupp, S. I. *Science* **1996**, *380*, 325.
(12) Trindade, T.; O′Brien, P.; Zhang, X. M. *Chem. Mater.* **1997**, *9*, 523.
(13) Beecroft, L. L.; Ober, C. K. *Chem. Mater.* **1997**, *9*, 1302.
(14) Ozin, G. A. *Adv. Mater.* **1992**, *4*, 612.
(15) Hofman-Caris, C. H. M. *New J. Chem.* **1994**, *18*, 1082.
(16) Bats, F. S. *Science* **1991**, *251*, 898.
(17) Douy, A.; Gallot, B. *Makromol. Chem.* **1973**, *165*, 297.
(18) Thomas, E. L.; Kinning, D. L.; Alward, D. B.; Henkee, C. S. *Macromolecules* **1987**, *20*, 2934.
(19) Thomas, E. L.; Alward, D. B.; Kinning, D. J.; Martin, D. S.; Handlin, Jr. D. L.; Fetters, L. J. *Macromolecules* **1986**, *19*, 2197.
(20) Sankara, V.; Cummins, C. C.; Schrock, R. R.; Cohen, R. E.; Silbey, R. J. *J. Am. Chem. Soc.* **1990**, *112*, 6858.
(21) Cummins, C. C.; Schrock, R. R.; Cohen, R. E. *Chem. Mater.* **1992**, *4*, 27.
(22) Sankaran, V.; Yue, T.; Cohen, R. E.; Schrock, R. R.; Sillbey, R. S. *Chem. Mater.* **1993**, *5*, 1133.
(23) Tuzar, Z.; Kratochvil, P. *Adv. Colloid, Interface Sci.* **1976**, *6*, 201.
(24) Noolandi, J.; Hong, K. M. *Macromolecules* **1983**, *16*, 21443.
(25) Gast, A. P. *Scientific Methods for the Study of Polymer Colloids and Their Applications;* Kluver: Dordrecht, 1990; Vol. 2, pp 311−328.

10.1021/cm980613z CCC: $18.00
Published on Web 01/23/1999

vinylpyridine),[26] poly(4-vinylpyredine),[27] poly(ethylene oxide),[28] poly(acrylate),[29] poly(methylacrylate), and poly(acrylic acid)[30] have been applied to synthesize nanocomposites containing a wide range of metallic and semiconducting nanocrystals. The precursors of the desired nanocrystals can be introduced into the micelle cores directly as metallic ions [26,27,29] or indirectly as counterions.[28,30]

From the point of view of materials science, producing composites with specific electronic and optical properties is of great importance, these properties are largely determined by the size of metallic or semiconducting nanocrystals within polymer matrixes. The size of nanocrystals within polymers are controlled mostly by the polymer composition. The control of the composition of block copolymers can be achieved by use of well-established techniques of sequential living polymerization.[31] However, the harsh polymerization terms and the limited selection of monomers in living polymerization technique have thrown obstacles in the size control of inorganic nanocrystals in the block copolymer micelle. In this article, based on the stability of the block copolymer micelle, we have developed a size-control technique of inorganic nanocrystals, in which the size of nanocrystals was controlled simply by repeating the synthesis procedure for a definite number of cycles carried out within block copolymer micelle. By this method, we have prepared a series of CdS nanocrystals with different sizes in hydroxylated poly(styrene-*b*-butadiene-*b*-styrene) (HO-SBS) micelle. In addition, the electron process of the resulting nanocomposites have been investigated with surface photovoltage spectroscopy (SPS) and electric field induced surface photovoltage spectroscopy (EFISPS).

2. Experimental Section

2.1. Materials. The poly(styrene-*b*-butadfiene-*b*-syrene) (SBS) is a commercial block copolymer manufactured by Baling Oil Chemical Industry Company (Yueyang, China). Its mean molecular weight is 139 000, and its weight fraction of polystyrene (PS) blocks is 40%.

2.2. Hydroxylation of SBS. In a typical hydroxylation run,[32] 10 g of SBS was dissolved in 100 mL of chloroform in a 500-mL three-neck glass flask equipped with a condenser, a mechanical stirrer, and a thermometer. Then 100 mL of formic acid and 10 mL of peroxide hydrogen were added into the flask. The reactant solution was stirred for 1 day at 50 °C. After the completion of the reaction, the polymer was coagulated in petroleum ether and was purified by recoagulating twice. The coagulated polymer was then dried at 40 °C under a vacuum. Its hydroxyl value is measured to be about 0.36 with the acidation method[33] and its structure were determined by infrared (IR) spectroscopy (Nicolet 5PC).

Table 1. Dependence of CdS Nanocrystal Size on the Cd Content and Repeating Times in the Resulting Nanocomposites

	nanocomposite		
sample	I	II	III
repeating times	1	2	4
Cd (g/g) calcd[a]	0.4	0.8	1.6
Cd (g/g) expt	0.3	0.7	1.3
average size (nm)[b]	2.8	5.0	9.7

The values were calculated based on the HO value of HO-SBS. These sizes were determined by TEM images of the resulting nanocomposites.

2.3. Preparation of CdS/HO-SBS Nanocomposites. The resulting hydroxylated polymer, referred to as HO-SBS, was dissolved in toluene to form the solution with concentration of 1% (weight/volume). The anhydrous $CdCl_2$ was added into the solution. Its solubilization was facilitated by means of ultrasound, and then Na_2S was introduced into the solution saturated by $CdCl_2$. After the extracting of NaCl with H_2O from the reaction mixture, a pale yellow solution was obtained and the nanocomposite I was prepared. Repeating the procedure above for 2 and 4 times, the nanocomposite II and nanocomposite III were prepared, respectively. The color of the resulting solutions was transformed from yellow to red gradually with the increase of repeating times.

2.4. Characterizations of CdS/HO-SBS Nanocomposites. The contents of Cd^{2+} ions were determined by use of graphic furnace atomic absorption spectrophotometer (HITACHI 180−50), which were listed in Table 1.

Thin films of the resulting nanocomposites were obtained by putting a small drop with the polymer concentration of 1 mg/mL on a carbon-coated copper grid. These films were studied by means of transmission electron microscopy (TEM) (bright field images, HITACHI, H-81001V, 200 KV).

The X-ray diffraction patterns of the resulting nanocomposites were obtained on a Rigaku D/max rA Diffractometer using the Cu Kα line as radiation ray.

The absorption spectra of the resulting solution were measured on a spectrophotometer (UV-240, Shimadzu).

SPS was measured on a home-built apparatus. The surface photovoltage effect, which consists of a change at the surface potential barrier caused by illumination, has been applied successfully to the investigation of the electron processes in semiconductors.[34] The generation of photovoltage arises from the creation of electron−hole pairs, followed by the separation under a built-in electric field (the space-charge layer). The former requires the semiconductors with a suitable band gap. The latter needs that the electron−hole pairs can be separated and transported to electrode surface efficiently under a consider strong built-in electric field.

(26) Spatz J. P.; Roescher, A.; Sheiko, S.; Kransch, G.; Möller, M. *Adv, Mater.* **1995**, *7*, 731
(27) Autonientti, M.; Wenz, E.; Bronstem, L..; Seregina, M. *Adv. Mater.* **1995**, *7*, 1000.
(28) Spartz, J. P.; Roescher, A.; Möller, M. *Adv. Mater.* **1996**, , 337.
(29) Moffitt, M.; McMahon, L.; Pessel, V.; Eisenberg, A. *Chem. Mater.* **1995**, *7*, 1185.
(30) Moffitt, M.; Eisenberg, A. *Macromolecules* **1997**, *30*, 4363.
(31) Noshay, A.; McGrath, J. K. *Block Copolymers: Overview and Critical Survey*; Academic Press: New York, 1977.
(32) Wang, B. R. *Organic Synthesis Reactions*; Science Press: Beijing, 1982; p 60 (in Chinese).
(33) Braun, D.; Cherdron, H.; Kern, W. *Practical Macromolecular Organic Chemistry* (trans from German by Ivin, K. J.) 3rd rev. and enlarged ed.; Harwood Academic Publishers: 1984; p 244. (MMI Press: Polymer Monograph Series; Elias, H.-G., Ed.; Vol. 2).
(34) Wang, D. J.; Liu, W.; Xiao, L. Z.; Li, T. J. *Chemistry* (in Chinese) **1989**, *10*, 32.

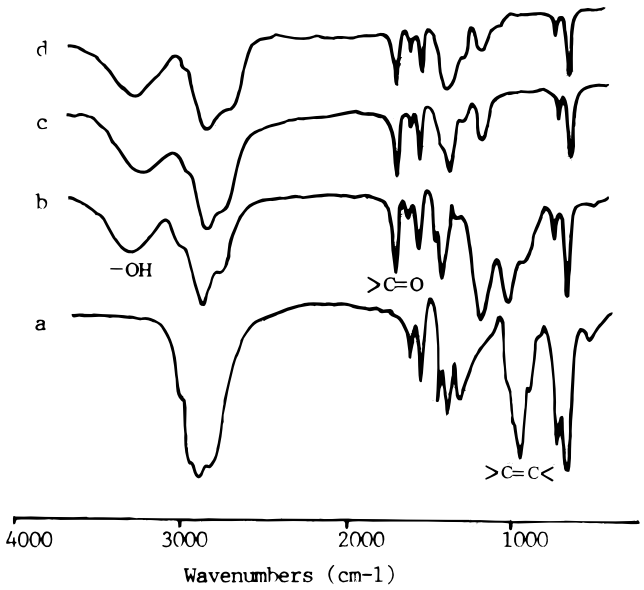

Figure 1. IR spectra of SBS (a), HO-SBS (b), HO-SBS loading Cd^{2+} (c), and CdS/HO-SBS nanocomposites (d).

Scheme 1. Molecular Structure of the Resulting HO-SBS

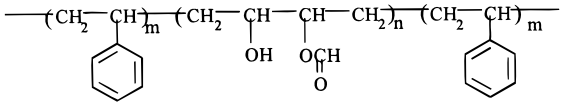

SPS measurements are carried out with a solid-junction photovoltaic cell indium tin oxide (ITO)/sample/ITO, a light source, a monochromator and a lock-in detection technique. Monochromatic light is obtained by passing light from a 500-W Xenon lamp through a double-prism monochromator (Higher and Watts, D300). A lock -in amplifier (Brookdeal, 9503-SC), synchronized with a light chopper, is used to amplify the photovoltage signal.

EFISPS is a technique which combines the field effect principle with SPS. The external bias is applied to the two sides of the sample and is regarded as positive when the side under illumination is connected to a positive electrode.[35]

3. Results and Discussion

3.1. Structure Characteristics of CdS/HO-SBS Nanocomposites. Compared with the IR spectrum of the pure SBS (Figure 1a), the band at 967 cm^{-1} corresponding with the in-plane rocking vibration of double bonding of poly(*trans*-1,4-butadiene) units completely disappeared, and the two bands were observed at about 3424 and 1720.7 cm^{-1} (Figure 1b), which are due to the stretching vibrations of OH groups and carbonyl groups, respectively. This suggested that most double bonding of PB blocks was hydroxylated. The molecular structure of the resulting HO-SBS was shown in Scheme 1.

In nonpolar solvents, e.g., toluene, HO-SBS molecules with nonpolar PS blocks and polar HO−PB blocks could self-organize into a nanosized micelle consisting of a PS shell and a HO−PB core. The HO−PB cores are capable of binding metallic ions, e.g., Cd^{2+}, so they may be regarded as nanoreactors to prepared nanoparticles. After loading with $CdCl_2$, the HO stretching vibration band of HO-SBS molecules moved to 3413 cm^{-1} and their carbonyl stretching vibration band did not change (Figure 1c). This indicated that the Cd^{2+} ions were introduced into the HO−PB core only through the coordination with HO groups, whereas the carbonyl groups did not take part in the coordination process. Upon coordination, the O−H bond is weakened and the HO stretching frequency is lower, so its stretching band is shifted to low wavenumbers from the value of the pure HO-SBS[36] shown in Figure 1b. After introduction of S^{2-} ions, the HO stretching band located at 3424 cm^{-1} again (Figure 1d). This implied that the HO groups in HO−PB cores were refreshed again after formation of CdS in a micelle, which gave an opportunity to prepare larger nanoparticles by repeating the above-mentioned synthesis procedure for a definite number of cycles. The Scheme 2 showed the synthesis procedure of nanoparticles in HO-SBS micelle.

As given in Table 1, with the increase of times of repeating the synthesis procedure, the Cd content in micelle increased. When repeating the synthesis cycle once, the Cd content of the resulting nanocomposite I was 0.3 g/g; twice, the Cd content of nanocomposite II was 0.5 g/g; 4 times, the Cd content of the nanocomposite III was 1.3 g/g. The Cd contents of the resulting nanocomposites were less than the calculated values based on the HO value of the HO-SBS and they did not increase in proportion to times of repeating synthesis cycle, which indicated that only some HO groups took part in the coordination with Cd^{2+} ions. It was the reason that tangling of polymer chains in the dense HO−PB cores decreased nucleation sites inside the cores and the formation of CdS particles in HO-SBS micelle also restricted in the reaction of the HO groups around the particles. In the CdS/HO-SBS nanocomposites, the nanometer dimension of HO−PB core imposed an upper limit on the size of the resulting CdS particles in the micelle, and the PS shell efficiently prevented them from aggregating. TEM images of all resulting composite films showed that the resulting CdS nanoparticles had no agglomeration (Figure 2). As given in Table 1, the average size of particles increased with the increase of the repeating times (Figure 2). CdS particles of the nanocomposite I were the smallest and their size was only 2.8 nm (Figure 2a). CdS particles in the nanocomposite II were 5.0 nm (Figure 2b). After repeating the synthesis cycle 4 times, CdS particles in nanocomposite III had grown to 9.7 nm (Figure 2c).

The X-ray diffraction patterns of composite III are given in Figure 3. Its principal diffraction peaks and Miller indices are at 2θ values of 26.55°, 43.91° and 51.85°, respectively, which agreed well with the corresponding peaks for cubic CdS (111, 220, and 311 reflections) listed in the standard reference table.[37] The diffraction peaks of CdS in either nanocomposite I or nanocomposite II were not perceived for their very low

(35) Zhang, J.; Wang, D. J.; Shi, T. S.; Wang, B. H.; Sun, J. Z.; Li, T. J. *Thin Solid Films* **1996**, *284−285*, 596.

(36) Nakamoto, K. *Infrared and Raman Spectra of Inorganic and coordination Compounds* 4th. ed.; John Wiley & Sons: New York, 1986; p 191.

(37) Powder Diffraction File ASTM, 1969 Card No. IO-454 and 6-0314 for cubic CdS.

Scheme 2. Synthesis Procedure of the Nanoparticles in HO-SBS Micelle

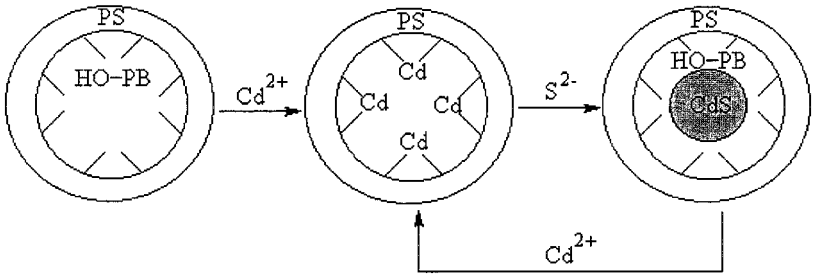

Cd content and were drowned by the polymer amorphous peaks.

In nanosized semiconductors, the de Broglie wavelength of electrons (or holes) becomes comparable to the crystallite size. The charge carriers have to be treated as quantum mechanically as "particles in box", where the size of the box is given by the dimension of the crystallites. The spacing between these energy levels and band gap strongly depends on the size of the nanocrystals. Many of their properties are size-tunable.[1−4]

Figure 4 showed the UV−vis, absorption spectra of the resulting composites. The absorption edge of 2.8-nm CdS nanocrystals in nanocomposite I was at approximately 480 nm and it was clearly blue-shifted from the bulk value of 515 nm (Figure 4a). As the size of CdS particles increased, the absorption edge was red-shifted to bulk value. The absorption edge of 5-nm CdS nanocrystals in the nanocomposite II was at approximately 490 nm (Figure 4b). In nanocomposite III, the value of 9.7-nm CdS was red-shifted to 505 nm (Figure 4c).

The same size-tunable phenomenon also was observed in SPS spectra of the resulting nanocomposites (Figure 5). The photovoltage response of 2.8-nm CdS nanocrystals in nanocomposite I was extremely weak because of the low Cd content (Figure 5a). In nanocomposite II, 5-nm CdS nanocrystals gave a threshold at about 474 nm, corresponding to the band gap of 2.61 eV, and a band-band transition at about 404 nm (Figure 5b). In nanocomposite III, the threshold of 9.7-nm CdS nanocrystals had red-shifted to 485 nm, corresponding to the band gap of 2.55 eV, and their band−band transition at 419 nm, respectively (Figure 5c).

3.2. Electron Process of CdS/HO-SBS Nanocomposites. The bulk cubic CdS is the photoconductor with a band gap of 2.4 eV. Its conduction band (E_C) and valence band (E_V) are at −4.1 eV and −6.5 eV, respectively, with respect to the vacuum energy level, and its Fermi level (E_F) is somewhat greater than −5.3 eV for no doping.[38] So far as the electric property is concerned, the polymer also can be considered as a semiconductor with the large band gap. To be easy to explain, only the PS shell is taken into account in the energy band model of the nanocomposite. The E_C, E_V, and E_F of PS are −2.5 eV, −7.1 eV, and −4.8 eV, respectively, and its band gap is 4.6 eV [39]. According to the above-mentioned data (the applicability of these values of bulk material for small particles was confirmed by recent studies[40]), the structure of the resulting nanocomposites (Scheme 2) and the SPS measurement cell structure (Scheme 3), an energy band model is given in Figure 6. There are heterojunctions at the CdS/PS interfaces and Schottky potential barriers at the PS/ITO interfaces in the model.

Under illumination, CdS nanocrystals within the nanocomposites could produce a lot of photogenerated electrons on E_C, whereas, photogenerated holes are left on E_V. A very high potential barrier exists at the CdS/PS heterojunctions, only a few electrons tunnel the PS shell into the lighted PS/ITO interface, because there is a series of traps representing the molecular folding, bond adjustment, and the protrusion of side and end groups in polymer,[39] which causes the increase of the surface barrier at the lighted interface. Benefiting by extremely high sensitivity of the SPS technique, the very small difference of the surface barrier between the lighted and dark PS/ITO interfaces was perceived and a very weak photovoltage response of CdS in nanocomposite I was obtained (Figure 5a). With the increase of the Cd content within the nanocomposites, more photogenerated electrons tunneled through PS shell and caused the stronger CdS photovoltage response (Figures 5b and 5c).

Taking nanocomposite III of the largest Cd content for example, the electric field induced electron process of such nanocomposites was investigated. The EFISPS spectra of nanocomposite III were shown in Figure 7. When an external positive bias (+1.0 V) was applied, its photovoltage response became very intense (Figure 7b). Whereas, when an external negative bias (−1.0 V) was applied, a negative photovoltage response was observed (Figure 7c).

When an external positive bias is applied (for example, +0.1V), the whole energy band will be tilt, the potential at the positive electrode is lower than that at the negative electrode (Figure 6). The wall of potential barrier at the CdS/PS heterojunctions becomes thinner also. In addition, the positive electric bias largely improves the electronic mobility in the PS shell.[39] This accelerates the photogenerated carrier tunneling in the PS shell. Therefore, under the positive electric bias, more photogenerated electrons tunnel the PS shell from left to right along the electric field direction and are accumulated in the trap (A) nearest to the lighted ITO/PS interface, whereas, the corresponding photogenerated holes are accumulated in the trap (B) nearest to the dark ITO/PS interface. Therefore, an charge separation is obtained in the whole energy band model. Eventually, a lot of electrons tunneled into the light PS/ITO interface under the electric field, caused the increase of the surface barrier of the interface, and

(38) Grätzel, M. *Heterogenerous Photochemical Electron Transfer;* CRC Press Inc.: Boca Raton, FL, 1989; p 101.
(39) Fabish, T. J.; Duke, C. B. *Polymer Surface*; Wiley-Interscience: Chichester, 1978; Chapters 4−6.
(40) Hässelbarth, A.; Eychmüller, A.; Weller, H. *Chem. Phys. Lett.* **1993**, *203*, 271.

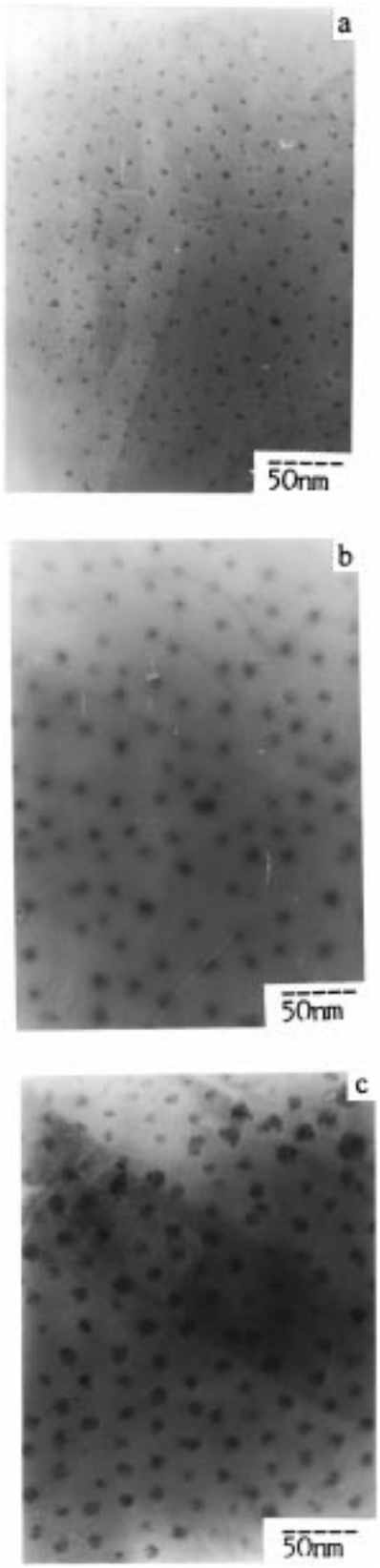

Figure 2. TEM images of nanocomposite I (a), nanocomposite II (b), and nanocomposite III (c).

resulted in a stronger photovoltage response than that without the external positive bias (Figure 7b).

When an external negative electric bias is applied (for example, −1.0V), the tilt direction of the energy band is contrary to that shown in Figure 6. Under the negative electric field, the photogenerated holes are

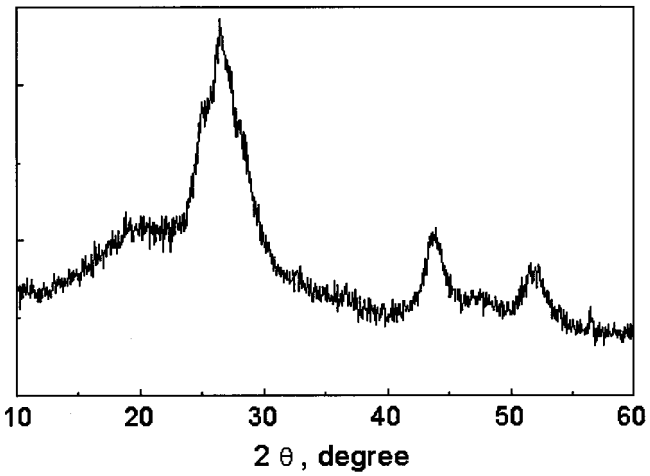

Figure 3. X-ray diffraction pattern of the nanocomposite III.

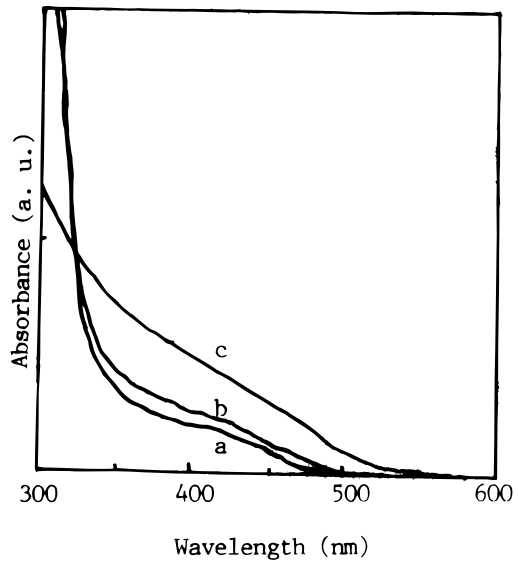

Figure 4. UV−vis spectra of nanocomposite I (a), nanocomposite II (b), and nanocomposite III (c).

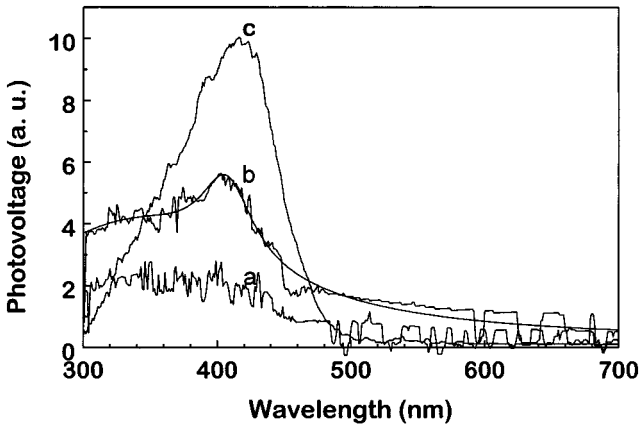

Figure 5. SPS spectra of nanocomposites I (a), nanocomposite II (b), and nanocomposite III (c).

accumulated in the trap nearest to the light ITO/PS interface (D) and the photogenerated electrons in the trap nearest to the dark ITO/PS interface (C). Eventually. The photogenerated holes tunnel the PS shell into the lighted ITO/PS interface and cause the decrease of the surface barrier of the interface. So the negative photovoltage response was observed (Figure 7c).

Scheme 3. Cell Structure for SPS Measurement

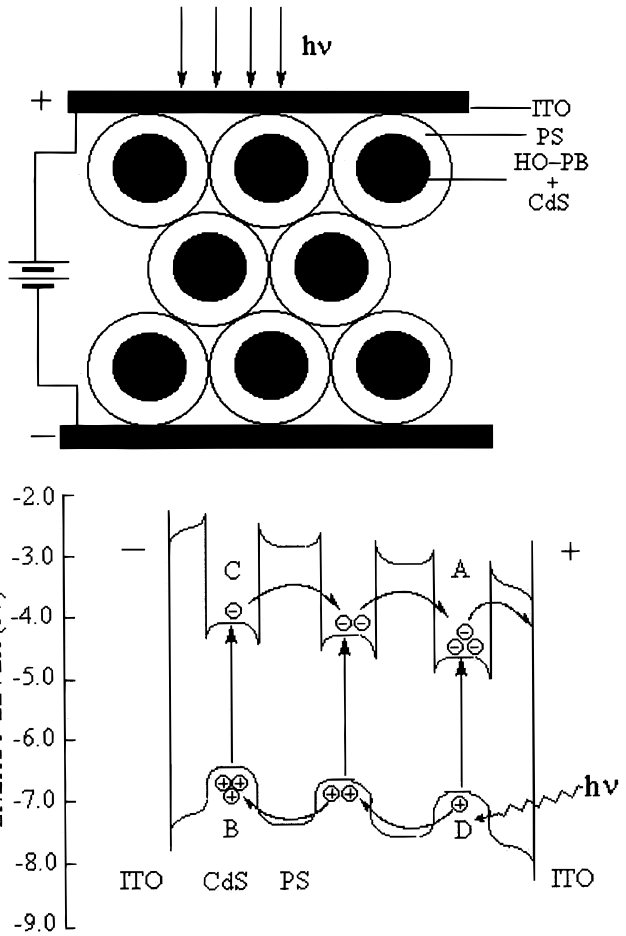

Figure 6. The energy band model of the resulting composite under an external positive bias (all energy levels were given vs vacuum energy level).

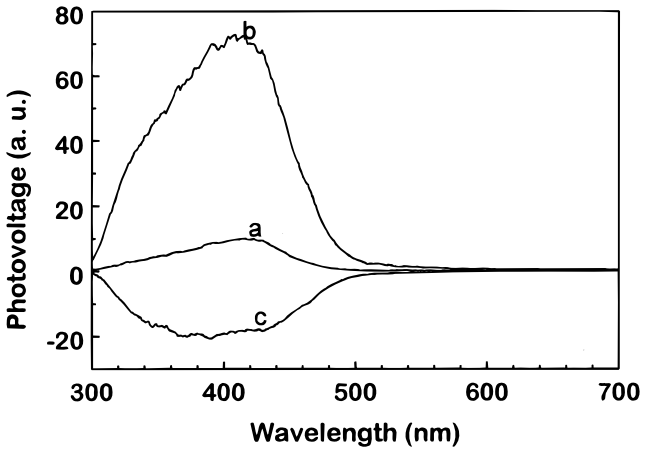

Figure 7. EFISPS spectra of nanocomposite III: 0.0 V (a), +1.0 V (b), and −1.0 V(c).

Based on the energy band model (Figure 6), it is predicted that the high potential barrier at the CdS/polymer heterojunctions could prevent the recombination of photogenerated carriers and maintain the charge separation in the nanocomposite for a period. Figure 8 showed the decay curve of the CdS photovoltage response value with time after removal of the external positive bias. The CdS photovoltaic value is 0.42 μV without the external positive bias ($t = 0$ min). After an external positive bias (+ 1.95V) was applied, the CdS

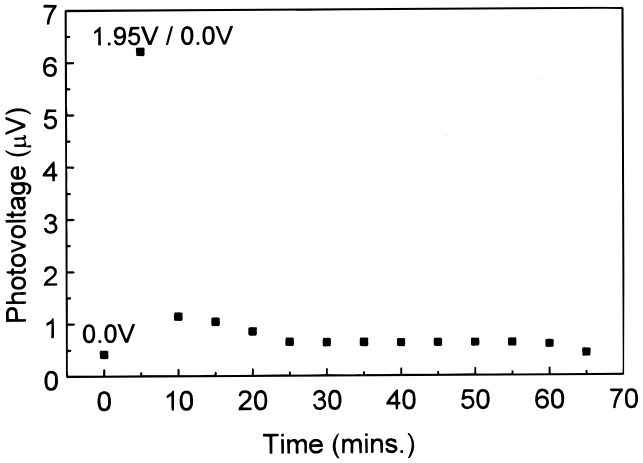

Figure 8. The SPS decay curve of nanocomposite III with time after removal of the external bias (+1.95V).

photovoltaic value rose to 6.21 μV ($t = 5$ min). As soon as the external bias was removed, the CdS photovoltaic value decreased quickly. In 5 min, the value had declined to 1.14 μV ($t = 10$ min). Since then the decrease rate of the CdS photovoltaic value slowed and leveled off to about 0.65 μV ($t = 25$ min). After 40 min, the CdS photovoltaic value returned gradually to 0.43 μV ($t = 65$ min).

As the external bias is removed, the whole energy band is likely to be returned to the original balance state model without the external bias. So the separated photogenerated electrons and holes quickly will tunnel the polymer layer in the opposite directions and recombine, and the CdS photovoltaic value will decrease quickly. Because the high potential barriers at the CdS/PS heterojunctions result in the deep electron traps on E_C and the deep hole traps on E_V in the energy band model and the electronic mobility in the PS shell decreases largely after removal of the external bias, the tunneling and recombination of the separated carriers is restricted to some extent and the CdS photovoltage response is perceived in a certain period, although it become weaker and weaker. The plateau value of the CdS photovoltage response (0.65 μV) given in Figure 8, which is larger than the value without the external bias (0.42 μV), implied that deep electron traps on E_C and deep hole traps on E_V in the energy band model can storage some photogenerated electrons and holes for a certain period, this will be more significant to photoelectron information storage. The work on this study is in progress.

4. Conclusion

HO-SBS molecules formed a micelle consisting of a PS shell and a HO-PB core in toluene. With such micelles as nanoreactors, a series of CdS nanocrystals with different sizes simply through repeating the synthesis procedure for a definite number of cycles have been prepared. As the Cd content of the resulting nanocomposites increased, the size of CdS nanocrystals increased, their absorption edge, the SPS threshold and band-band transition were red-shifted to bulk value.

Based on the SPS and EFISPS spectra of the resulting nanocomposites, a reasonable energy band model was proposed to describe the electron process in the nano-

composites. There was a plateau value of the CdS photovoltage response in the decay curve with time after removal of the external bias. This was due to the high potential barrier of the polymer shell which can prevent the recombination of separated charges.

Clearly, repeating the synthesis procedure for a defined number of times may provide a controlled route to the stepwise chemical construction of nanocrystals with tunable size. Such composites have shown great promise in hybrid materials and information storage and processing.

CM980613Z